Available online at www.sciencedirect.com
ScienceDirect
Precambrian Research 154 (2007) 107–124
Precambrian Research
www.elsevier.com/locate/precamres

LA-ICP-MS U–Pb zircon geochronology and geochemistry of Paleoproterozoic mafic dykes from western Shandong Province: Implications for back-arc basin magmatism in the Eastern Block, North China Craton

Yuejun Wang [a,c,*], Guochun Zhao [b], Weiming Fan [a], Touping Peng [a], Linhua Sun [a], Xiaoping Xia [b]

[a] *Key Laboratory of Isotope Geochronology and Geochemistry, Guangzhou Institute of Geochemistry, Chinese Academy of Sciences, Guangzhou 510640, China*
[b] *Department of Earth Sciences, The University of Hong Kong, Pokfulam Road, Hong Kong, China*
[c] *Department of Earth Sciences, Northwest University, Xi'an 710069, China*

Received 21 August 2006; received in revised form 10 December 2006; accepted 22 December 2006

Abstract

LA-ICP-MS U–Pb zircon geochronological, elemental and Sr–Nd isotopic data are presented for Paleoproterozoic mafic dykes in western Shandong Province to characterize the Paleoproterozoic tectonic process in the Eastern Block, North China Craton. These dykes are predominantly dolerite with a major mineral assemblage plagioclase + clinopyroxene and yield a LA-ICP-MS U–Pb zircon age of 1841 ± 17 Ma. They are geochemically low- to medium-potassium subalkaline basalts and basaltic andesites. ($^{87}Sr/^{86}Sr$)(i) ratios range from 0.702859 to 0.703706, and $\varepsilon_{Nd}(t)$ values are from +3.82 to +7.42, which are slightly enriched comparable to a MORB source. The arc-like signatures are revealed in these dykes by the enrichment in LILEs and LREEs and depletion in HFSEs and HREEs. Such signatures suggest an origination from a MORB-like source metasomatized by newly subduction-related fluids potentially via source contamination. The geochemical affinity to both MORB- and arc-like sources, together with incompatible elemental ratios (e.g., Zr/Y, Th/Yb, Ta/Yb, Th/Nb and Ba/La), appears to support a development of a Paleoproterozoic intra-continental extension or failed back-arc basin setting within the Eastern Block in response to an upwelling asthenosphere, accompanied by the amalgamation of the Western and Eastern Blocks along the Trans-North China Orogen at ∼1.85 Ga. Such a proposed tectonic setting might be analogue to modern back-arc basins along the western Pacific.

Keywords: Paleoproterozoic mafic dykes; LA-ICP-MS zircon dating; Elemental and isotopic geochemistry; Intra-continental back-arc basin; Eastern Block; North China Craton

1. Introduction

The North China Craton (NCC) is the largest and oldest known cratonic block in China. A major achievement in understanding the history of the craton has been made following recognition of a Paleoproterozoic collisional belt, referred to as the Trans-North China Orogen

* Corresponding author at: Guangzhou Institute of Geochemistry, Chinese Academy of Sciences, P.O. Box 1131, Guangzhou 510640, China. Tel.: +86 20 85290527; fax: +86 20 85290151.
E-mail address: yjwang@gig.ac.cn (Y. Wang).

0301-9268/$ – see front matter © 2007 Elsevier B.V. All rights reserved.
doi:10.1016/j.precamres.2006.12.010

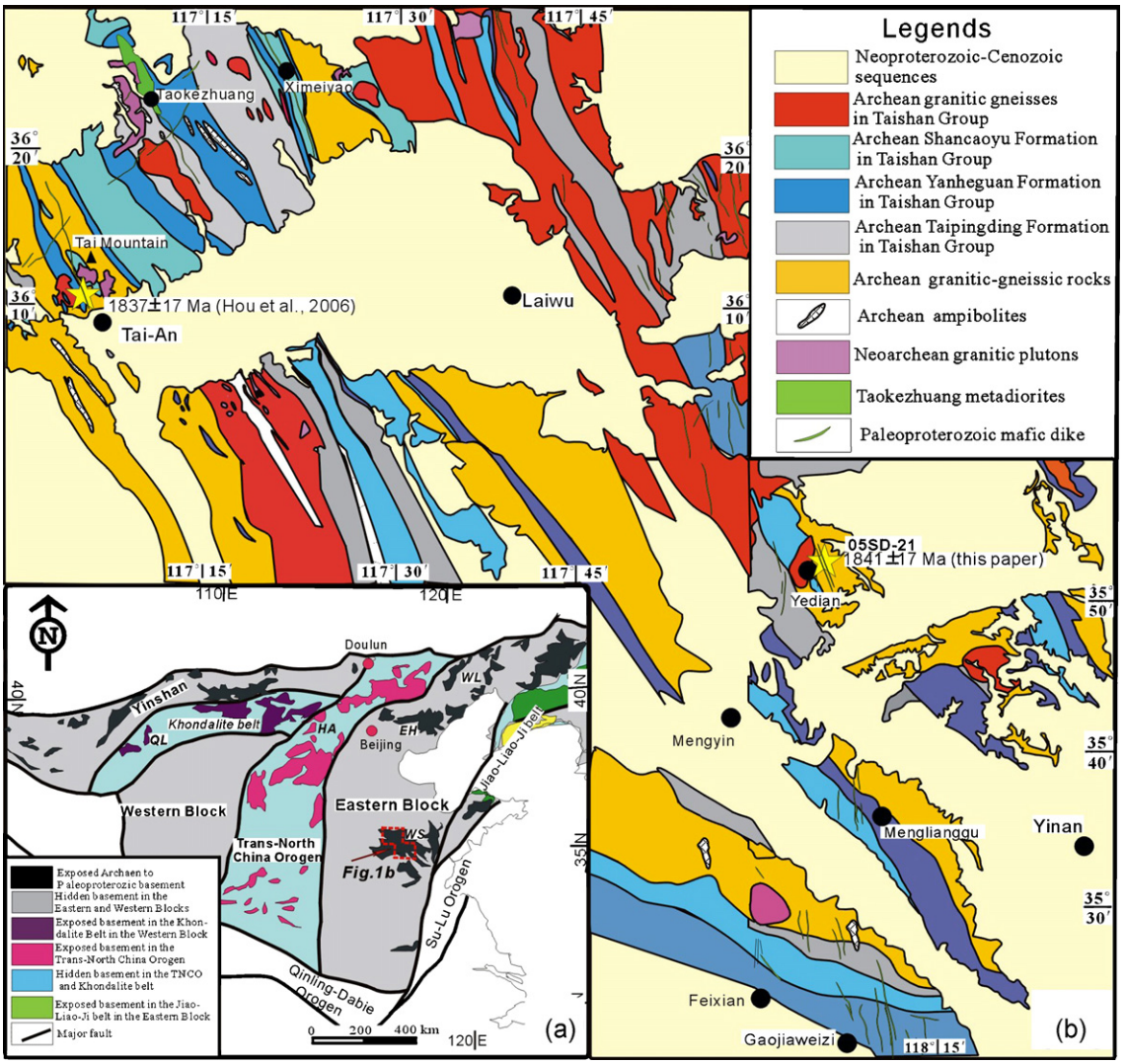

Fig. 1. (a) Skeptical map of the North China Block (NCC) with a three-fold subdivision (after Zhao et al., 2005); (b) geological map of the Tai'an-Laiwu-Mengyin-Feixian areas showing the distribution of Paleoproterozoic mafic dykes (after SDBGMR, 1991).

(TNCO) along which two discrete continental blocks, named the Eastern and Western Blocks (Fig. 1a), collided to form the NCC (Zhao et al., 1998, 1999, 2000, 2001, 2002a,b; Wilde et al., 2002). There is now a coherent outline of the timing and tectonic processes involved in the Paleoproterozoic amalgamation and much intensive knowledge concerning the pre-collisional history of the craton has been advanced (Kröner et al., 1998, 2006; Zhao et al., 1999, 2000, 2002a,b, 2003; Guo et al., 2002; Liu et al., 2002, 2004, 2005, 2006; Zhai and Liu, 2003; Wang et al., 2003). However, the tectonic histories of the Paleoproterozoic rocks in the interiors of the Eastern and Western Blocks are still poorly understood.

Paleoproterozoic mafic dykes are extensively distributed in the TNCO, but they also occur within the Eastern and Western Blocks. Theses dykes can provide important information on the nature of lithospheric of the NCC and its Paleoproterozoic tectonic evolution. Recent studies have mainly focused on the unmetamorphosed mafic dykes in the TNCO (e.g., Qian and Chen, 1987; Wang et al., 2004, in press). The available results show that these dike swarms in the TNCO were emplaced at 1765–1781 Ma (Wang et al., 2004; Peng et al., 2005; Halls et al., 2000), and were the derivations of heterogeneously subduction-modified lithospheric sources in response to the orogenic collapse (Wang et al., 2004, in press). However, little attention has been paid to small-voluminous mafic dykes in the Eastern and Western Blocks. It is also poorly known whether the emplacement of the mafic dykes in the two blocks were coeval

with those in the TNCO. Hou et al. (2005, 2006) recently reported that diabasic dykes from the Taishan and Laiwu areas (western Shandong Province) of the Eastern Block were emplaced at age of 1837–1887 Ma using SHRIMP U–Pb zircon dating technique, earlier than those in the TNCO, and suggesting that they may not have been related to a post-collisional extensional event as those in the TNCO. However, more precisely geochronological data and systematically geochemical investigations for these dykes in the eastern Block are still rare so far. It still remains unknown about the tectonic nature of the Paleoproterozoic mafic dykes in the Eastern Block. In this study, we carried out geochronogical, elemental and Sr–Nd isotopic investigations on these mafic dykes in order to determine their emplacement time, petrogenesis and tectonic setting, and then to provide important insights into understanding of the Paleoproterozoic evolution of the NCC.

2. Geological background

The basement of the NCC can be divided into the Eastern and Western Blocks, separated by the TNCO (Fig. 1a; Zhao et al., 1999, 2003). Detailed lithological, geochemical, structural, metamorphic and geochronological differences between the Eastern and Western Blocks and the TNCO and their possible tectonic evolution have been summarized by Zhao et al. (2001, 2005).

As one of the largest basement exposure in the Eastern Block in the NCC, the Western Shandong Complex encompasses more than 15,000 km^2 and is bounded by the Qishu fault to the east and by the Liaocheng–Lankao fault to the west (see SDBGMR, 1991). To the east of the Eastern Block there occurred Paleoproterozoic granitic, bimodal volcanic and sedimentary rocks (Liu et al., 2004; Zhao et al., 2005 and references therein) whereas to the west a Paleoproterozoic active-type continental margin was developed (Zhao et al., 1999, 2001, 2005). In this complex, the basement rocks consists of Archaean ultramafic to felsic igneous rocks and minor supracrustal rocks (e.g., komatiite, basalt and high-Al tonalitic–trondhjemitic–granodioritic (TTG) gneisses) that are the representative of Archaean granite–greenstone belts in China (Xu et al., 1992; Cao et al., 1996; Polat et al., 2006; Liu et al., 1992; Jahn et al., 1988). These rocks were intruded by ~2.55 Ga granites and charnockites (Jahn and Zhang, 1984; Jahn et al., 1988; Kröner et al., 1998) and unmetamorphosed Paleoproterozoic mafic dykes (e.g., SDBGMR, 1991).

Associated with the granite–greenstone sequence in the Complex is Paleoproterozoic mafic dykes that are dominantly distributed in the Tai'an-Laiwu-Mengyin-Feixian areas (Fig. 1b). These dykes intrude both the Archaean and Paleoproterozoic basements, and are unconformably overlain by the Neoproterozoic to lower Cambrian sedimentary sequences (SDBGMR, 1991; Qian and Chen, 1987; Hou et al., 2005, 2006). Most of these dykes generally strike NW-NWN with a steeply dipping angle and a few exhibits a NE-NNE trending (Fig. 1b). Their thickness ranges from less than half a meter to 2–5 m and length from 5 to 500 m (with several up to 2000 m). Mapped length of individual dykes is commonly in range of 5–20 km. They occur as dykes and stocks and are commonly free of deformation and metamorphism. Low-temperature alteration is occasionally observed, as indicated by chlorite after pyroxene and calcite after plagioclase. Most of these dykes are lithologically dolerite with doleritic textures. The most common mafic mineral is augite (20–35% in volume), partially altered to chlorite and amphibole, and the predominant felsic phase is plagioclase (40–60% in volume) with andesine-labradorite composition. Plagioclase occurs both as phenocrysts and in the groundmass. Other minerals include amphibole (3–5%), biotite (~3%), quartz (2–4%), Fe–Ti oxides (1–2%) and minor amounts of euhedral titanite and apatite. Secondary chlorite is also usually observed.

3. Sample descriptions and analytical methods

In this study, the representative samples were collected from the Yedian (Mengyin County), Menglianggu (Mengyin County) and Gaojiaweizi (Feixian County) as shown in Fig. 1b, respectively. They are fresh doleritic dykes and have insignificantly deformational and metamorphic signatures. All samples have a similar mineral assemblage plagioclase + clinopyroxene + biotite + quartz ± amphibole, with minor chlorite and epidote.

Zircons were separated from sample 05SD-21 using the conventional heavy liquid and magnetic techniques and purified by handpicking under a binocular microscope. They were mounted on adhesive tape, enclosed in epoxy resin and polished, and then photographed in reflected and transmitted light. The internal structure of zircons was examined using the cathodoluminescence image technique prior to U–Pb isotopic analyses via a scanning electron microprobe at the Guangzhou Institute of Geochemistry (GIG), Chinese Academy of Sciences (CAS). The U–Pb isotope compositions of zircons were analyzed using a VGPQ-Excel ICP-MS with 213 nm Nd-YAG laser ablation system (USA) at the University of Hong Kong. The instrumental setting and detailed analytical procedure have been described by

Table 1
LA-ICP-MS U–Pb zircon analyses for Paleoproterozoic mafic dykes (05SD-21) from Western Shandong, Eastern Block

Spot	Pb_{rad}	^{232}Th	^{238}U	Th/U	Isotopic ratios						Apparent age (Ma)		
					$^{207}Pb/^{206}Pb$	1σ	$^{207}Pb/^{235}U$	1σ	$^{206}Pb/^{238}U$	1σ	$^{207}Pb/^{206}Pb$ ($\pm1\sigma$)	$^{207}Pb/^{235}U$ ($\pm1\sigma$)	$^{206}Pb/^{238}U$ ($\pm1\sigma$)
05SD-21-2	146.1	470.1	551.2	0.85	0.11250	0.00166	4.02865	0.05800	0.25972	0.00132	1840 ± 26	1640 ± 12	1488 ± 7
05SD-21-3	180.9	593.2	598.9	0.99	0.11374	0.00156	4.63982	0.06226	0.29587	0.00136	1860 ± 25	1756 ± 11	1671 ± 7
05SD-21-4	212.3	381.3	620.2	0.61	0.11332	0.00154	5.23851	0.07008	0.33528	0.00154	1853 ± 24	1859 ± 11	1864 ± 7
05SD-21-5	119.0	840.4	677.6	1.24	0.11292	0.00164	2.67881	0.03798	0.17205	0.00084	1847 ± 26	1323 ± 10	1023 ± 5
05SD-21-6	159.6	351.1	565.6	0.62	0.11085	0.00154	4.22506	0.05778	0.27644	0.00130	1813 ± 25	1679 ± 11	1573 ± 7
05SD-21-7	135.1	275.4	525.9	0.52	0.11389	0.00164	3.95238	0.05566	0.25170	0.00124	1862 ± 26	1624 ± 11	1447 ± 6
05SD-21-9	157.0	321.6	539.5	0.60	0.11089	0.00158	4.35835	0.06084	0.28506	0.00140	1814 ± 26	1704 ± 11	1617 ± 7
05SD-21-10	152.4	283.3	536.0	0.53	0.11295	0.00162	4.33623	0.06112	0.27844	0.00138	1847 ± 26	1700 ± 12	1584 ± 7
05SD-21-11	84.2	151.1	259.3	0.58	0.11200	0.00156	4.91262	0.06736	0.31813	0.00152	1832 ± 25	1804 ± 12	1781 ± 7
05SD-21-12	142.8	528.5	569.2	0.93	0.11186	0.00162	3.79034	0.05336	0.24577	0.00120	1830 ± 26	1591 ± 11	1417 ± 6
05SD-21-14	102.3	227.7	316.0	0.72	0.11387	0.00160	4.97802	0.06882	0.31708	0.00154	1862 ± 25	1816 ± 12	1775 ± 8
05SD-21-16	202.2	317.8	633.0	0.50	0.11340	0.00156	4.89356	0.06592	0.31297	0.00144	1855 ± 25	1801 ± 11	1755 ± 7
05SD-21-17	136.5	263.6	408.1	0.65	0.11320	0.00158	5.11542	0.07012	0.32774	0.00156	1851 ± 25	1839 ± 12	1827 ± 8
05SD-21-18	134.8	442.5	571.6	0.77	0.11279	0.00160	3.59162	0.04984	0.23095	0.00112	1845 ± 25	1548 ± 11	1339 ± 6
05SD-21-21	65.7	122.6	171.5	0.71	0.11197	0.00308	5.31021	0.11656	0.34397	0.00398	1832 ± 49	1871 ± 19	1906 ± 19
05SD-21-22	139.7	951.4	979.4	0.97	0.11161	0.00306	1.04043	0.02270	0.06761	0.00078	1826 ± 49	724 ± 11	422 ± 5
05SD-21-23	97.7	320.5	299.8	1.07	0.11287	0.00310	4.55614	0.10010	0.29277	0.00340	1846 ± 49	1741 ± 18	1655 ± 17
05SD-21-25	121.8	780.4	824.1	0.95	0.11113	0.00312	2.68629	0.06100	0.17532	0.00206	1818 ± 50	1325 ± 17	1041 ± 11
05SD-21-26	173.9	614.3	612.4	1.00	0.11158	0.00308	3.92364	0.08676	0.25504	0.00296	1825 ± 49	1619 ± 18	1464 ± 11
05SD-21-27	101.3	413.5	441.0	0.94	0.11091	0.00316	3.15551	0.07292	0.20636	0.00246	1814 ± 51	1446 ± 18	1209 ± 15
05SD-21-29	23.6	83.9	65.4	1.28	0.11097	0.00346	4.96823	0.13074	0.32472	0.00428	1815 ± 56	1814 ± 22	1813 ± 13
05SD-21-30	100.1	210.4	255.2	0.82	0.11192	0.00316	5.43948	0.12454	0.35250	0.00420	1831 ± 50	1891 ± 19	1947 ± 21
05SD-21-33	97.1	205.6	269.9	0.76	0.11265	0.00308	5.01633	0.10914	0.32299	0.00372	1843 ± 49	1822 ± 18	1804 ± 20
05SD-21-35	101.5	242.9	268.5	0.90	0.11196	0.00310	5.24208	0.11602	0.33959	0.00396	1831 ± 49	1859 ± 19	1885 ± 18
05SD-21-37	111.6	97.5	276.1	0.35	0.11303	0.00322	5.65818	0.13052	0.36307	0.00436	1849 ± 51	1925 ± 20	1997 ± 19
05SD-21-38	135.2	218.3	422.9	0.52	0.11412	0.00318	4.51911	0.10084	0.28722	0.00336	1866 ± 49	1734 ± 18	1628 ± 17
05SD-21-39	109.8	366.4	585.1	0.63	0.11098	0.00308	2.57848	0.05738	0.16852	0.00196	1816 ± 50	1295 ± 16	1004 ± 11
05SD-21-40	74.5	120.7	213.0	0.57	0.11282	0.00320	4.88958	0.11202	0.31433	0.00376	1845 ± 50	1800 ± 19	1762 ± 18

Table 2
Major and trace element abundances of Paleoproterozoic mafic dykes from Western Shandong, Eastern Block

Sample	Yedian (Mengyin)						Menglianggu (Mengyin)			Gaojiaweizi (Feixian)						
	05SD-18	05SD-19	05SD-21	05SD-22	05SD-23	05SD-24	05SD-25	05SD-27	05SD-45	05SD-47	05SD-48	05SD-49	05SD-50	05SD-54	05SD-56	05SD-58
SiO_2	51.49	51.66	52.07	51.71	51.53	51.40	51.72	51.33	51.01	51.07	50.91	50.31	50.26	50.99	51.01	50.36
TiO_2	1.97	1.97	1.98	1.95	1.97	2.04	1.99	2.04	2.08	2.03	2.08	2.16	2.09	2.09	2.07	2.17
Al_2O_3	13.62	13.73	13.64	13.63	13.73	13.84	13.73	13.79	13.40	13.34	13.28	13.34	13.41	12.89	13.43	13.48
MgO	5.67	5.83	5.44	5.97	5.65	6.12	5.63	6.06	5.56	5.54	5.59	5.62	5.83	5.84	5.50	5.98
Fe_2O_3	3.79	4.02	3.40	3.31	3.77	3.38	3.55	3.63	3.19	3.36	3.40	3.62	3.91	3.44	4.16	3.61
FeO	6.95	6.75	7.30	7.35	6.90	7.40	7.20	7.20	8.20	7.80	7.85	8.05	7.40	8.20	7.20	8.20
CaO	7.25	7.15	7.34	7.17	7.55	6.29	7.30	6.76	9.28	9.51	9.30	9.55	10.10	10.08	9.57	8.21
K_2O	2.08	2.22	2.03	2.12	1.89	2.06	2.03	1.96	1.64	1.29	1.32	1.57	1.26	1.53	1.35	1.52
Na_2O	3.05	2.86	3.10	2.96	3.12	3.25	2.97	3.16	2.34	2.54	2.66	2.16	2.26	2.37	2.25	3.03
P_2O_5	0.24	0.24	0.25	0.23	0.24	0.24	0.23	0.24	0.24	0.23	0.24	0.24	0.22	0.27	0.24	0.24
MnO	0.17	0.18	0.19	0.18	0.18	0.18	0.18	0.18	0.18	0.18	0.18	0.19	0.18	0.17	0.18	0.18
LOI	3.47	3.03	3.01	3.19	3.21	3.54	3.19	3.37	2.63	2.88	2.94	2.95	2.93	2.10	2.81	2.78
Total	99.75	99.64	99.75	99.77	99.74	99.74	99.72	99.72	99.75	99.77	99.75	99.76	99.85	99.97	99.77	99.76
$Mg^{\#}$	0.50	0.50	0.49	0.51	0.50	0.51	0.49	0.51	0.47	0.48	0.48	0.47	0.49	0.48	0.47	0.48
Sc	30.8	29.2	27.7		29.9	28.2	29.3	29.7	30.4	28.5	30.2	30.8	29.5	38.5	27.5	30.6
V	290	284	270		270	253	270	275	274	279	268	279	300	307	279	299
Cr	208	215	192		218	194	202	184	201	194	200	214	225	235	200	205
Co	35.2	32.9	31.3		31.8	32.7	33.5	34.5	34.5	33.0	35.2	37.7	36.6	38.9	33.2	38.1
Ni	94	94	86		91	84	87	83	91	86	87	91	99	89	84	101
Ga	17.63	17.00	17.55		17.44	17.74	16.28	16.80	16.13	15.76	16.51	15.61	16.43	18.94	16.27	18.16
Rb	97.5	122	92.9		88.7	96.4	91.4	89.2	83.4	67.2	64.1	89.7	80.8	79.4	73.6	94.4
Sr	409	376	388		431	422	414	436	424	418	448	367	355	399	385	410
Y	17.71	17.36	18.72		18.02	18.91	17.35	18.61	16.97	16.93	17.74	17.51	16.80	17.93	18.00	18.09
Zr	126	122	130		130	135	127	135	127	126	128	123	121	133	130	126
Nb	13.31	12.92	13.92		13.06	14.04	12.83	13.80	12.46	12.42	13.21	12.56	12.19	12.84	13.32	13.06
Cs	2.72	3.40	2.06		2.59	2.88	2.92	3.20	3.98	2.34	2.02	1.99	1.49	1.74	1.83	3.80
Ba	631	587	657		615	633	617	647	424	385	427	420	318	388	376	420
La	22.70	22.07	25.97		23.40	25.45	23.48	22.41	21.84	20.29	22.45	21.92	19.16	22.55	22.53	22.33
Ce	50.48	48.16	53.93		50.82	55.18	50.41	53.91	48.88	46.65	49.85	46.94	44.00	46.25	48.70	49.46
Pr	6.68	6.26	7.10		6.68	7.14	6.80	7.27	6.19	5.97	6.54	6.27	5.78	6.64	6.37	6.42
Nd	28.12	26.90	30.82		29.05	31.05	27.74	30.32	26.55	25.50	27.12	26.53	25.55	25.53	27.84	27.91
Sm	5.49	5.12	5.59		5.29	5.71	5.32	5.77	5.06	5.01	5.38	5.07	4.72	5.08	5.21	5.18
Eu	2.01	2.04	2.25		2.07	2.22	2.02	2.25	1.71	1.70	1.78	1.77	1.64	1.79	1.80	1.87
Gd	4.95	4.72	5.17		4.87	5.14	4.81	5.30	4.70	4.37	4.81	4.70	4.42	4.60	4.71	4.71
Tb	0.70	0.68	0.72		0.71	0.74	0.66	0.74	0.68	0.66	0.67	0.66	0.65	0.70	0.69	0.67
Dy	3.65	3.41	3.72		3.51	3.57	3.57	3.80	3.49	3.25	3.56	3.47	3.29	3.30	3.46	3.57
Ho	0.67	0.67	0.71		0.67	0.71	0.66	0.71	0.63	0.62	0.65	0.68	0.61	0.62	0.68	0.70
Er	1.74	1.65	1.69		1.73	1.78	1.73	1.81	1.67	1.63	1.76	1.67	1.60	1.65	1.70	1.73
Tm	0.25	0.24	0.26		0.25	0.26	0.25	0.27	0.24	0.24	0.23	0.25	0.22	0.26	0.25	0.26
Yb	1.49	1.47	1.55		1.55	1.62	1.53	1.52	1.53	1.43	1.55	1.53	1.44	1.52	1.53	1.57
Lu	0.24	0.24	0.23		0.25	0.27	0.24	0.25	0.23	0.23	0.24	0.24	0.23	0.28	0.25	0.25
Hf	3.12	2.88	3.12		3.03	3.24	3.18	3.31	3.09	2.98	3.13	3.02	2.87	2.93	3.01	3.04
Ta	0.87	0.82	0.89		0.87	0.91	0.86	0.94	0.84	0.82	0.86	0.83	0.82	0.84	0.86	0.85
Pb	6.69	6.87	6.17		5.28	4.58	7.47	4.12	5.63	6.12	8.07	5.82	7.08	6.83	6.65	5.96
Th	3.38	3.32	3.53		3.29	3.51	3.37	3.46	3.19	3.10	3.36	3.24	3.05	3.11	3.37	3.15
U	0.97	1.22	0.93		0.91	1.04	0.90	0.97	0.85	0.82	0.90	0.83	0.82	0.81	0.89	0.84
Nb/Ta	15.30	15.76	15.64		15.01	15.43	14.92	14.68	14.83	15.15	15.36	15.13	14.87	15.29	15.49	15.36
(Nb/La)n	0.56	0.56	0.52		0.54	0.53	0.53	0.52	0.55	0.59	0.57	0.55	0.61	0.55	0.57	0.56
(Th/La)n	1.20	1.21	1.10		1.14	1.12	1.16	1.10	1.18	1.24	1.21	1.20	1.29	1.11	1.21	1.14
(Hf/Sm)n	0.82	0.81	0.80		0.82	0.81	0.86	0.82	0.88	0.86	0.84	0.86	0.87	0.83	0.83	0.84

$Mg^{\#}$ is *mg*-numbers (=Mg/(Mg +Fe) in atomic ratio).

Table 3
Sr and Nd isotopic compositions of Paleoproterozoic mafic dykes from Western Shandong, Eastern Block

Sample	Sm	Nd	Rb	Sr	$^{147}Sm/^{144}Nd$	$^{143}Nd/^{144}Nd \pm 2\sigma$	$^{87}Rb/^{86}Sr$	$^{87}Sr/^{86}Sr \pm 2\sigma$	$(^{87}Sr/^{86}Sr)i$	$\varepsilon_{Nd}(t)$	T_{DM}
05SD-19	5.12	26.90	121.60	375.9	0.115	0.511839 ± 7	0.938	0.728410 ± 15	0.703446	3.82	1.98
05SD-21	5.59	30.82	93.00	388.0	0.110	0.511958 ± 8	0.695	0.722021 ± 12	0.703524	7.42	1.83
05SD-21′	5.59	30.82	93.00	388.0	0.110	0.511939 ± 14	0.695	0.721829 ± 15	0.703332	7.06	1.80
05SD-23	5.29	29.05	88.71	431	0.110	0.511946 ± 12	0.596	0.720215 ± 13	0.704346	7.08	1.79
05SD-25	5.32	27.74	91.40	414.4	0.116	0.511963 ± 7	0.639	0.720727 ± 14	0.703706	6.05	1.86
05SD-47	5.01	25.50	67.22	418.4	0.119	0.511962 ± 7	0.466	0.716012 ± 13	0.703613	5.32	1.92
05SD-49	5.07	26.53	89.69	367.3	0.116	0.511966 ± 7	0.708	0.721823 ± 13	0.702979	6.17	1.85
05SD-58	5.18	27.91	94.37	409.9	0.112	0.511868 ± 6	0.667	0.720626 ± 14	0.702859	5.08	1.93

Chondrite uniform reservoir values, $^{147}Sm/^{144}Nd = 0.1967$, $^{143}Nd/^{144}Nd = 0.512638$, are used for the calculation. $\varepsilon_{Nd}(t)$ is calculated by assuming 1850 Ma. Sm, Nd, Rb, and Sr: ppm. 05SD-21′ is a duplicate analysis of 05SD-21.

Xia et al. (2004). Spot size in the range of 40–50 μm was used for data collection. U–Pb ages of zircons were calculated using $^{238}U = 1.55125 \times 10^{-10}$/a and $^{235}U = 9.8454 \times 10^{-10}$/a via the Isoplot/EX3.0 software (Ludwig, 2001). The CN92-2 zircons (1143 Ma) were used to determine the elemental discrimination that occurs during sputter ionization. The analytical results are listed in Table 1.

The samples for the whole rocks analyses were crushed to millimeter-scale chips, and then powdered to 200-mesh using an agate mill. Major elements were determined by X-ray fluorescence spectrometry at the Hubei Institute of Geology and Mineral Resource, the Chinese Ministry of Land and Resources. FeO content was analyzed by a wet chemical method. Trace element analyses were performed at the GIG, CAS, using PE-Elan 6000 inductively coupled plasma mass spectrometer (ICP-MS). The analytical procedure is similar to that described by Liu et al. (1996). The international standard BCR-1 was chosen to calibrate element concentrations of measured samples. The analytical precision is better than 5% for elements >10 ppm, less than 8% for those <10 ppm, and about 10% for transition metals. The analytical results for major and trace elements are presented in Table 2.

Sr and Nd isotopic ratios were measured by MC-ICP-MS at the GIG, CAS. The analytical procedures are the same as reported by Wei et al. (2002). The total procedure blanks are in the range of 200–500 pg for Sr and <50 pg for Nd. The mass fractionation corrections for Sr and Nd isotopic ratios were based on $^{86}Sr/^{88}Sr = 0.1194$ and $^{146}Nd/^{144}Nd = 0.7219$, respectively. The measured $^{87}Sr/^{86}Sr$ ratio of (NIST) SRM 987 standard and the $^{143}Nd/^{144}Nd$ ratio of the La Jolla standard are 0.710265 ± 12 (2σ) and 0.511862 ± 10 (2σ), respectively. $^{143}Nd/^{144}Nd$ and $^{147}Sm/^{144}Nd$ ratios of CHUR at the present time used for calculating ε_{Nd} value are 0.512638 and 0.1967, respectively. $^{87}Rb/^{86}Sr$ and $^{147}Sm/^{144}Nd$ ratios were calculated using the Rb, Sr, Sm and Nd abundances measured by ICP-MS. The measured and age-corrected $^{87}Sr/^{86}Sr$ and $\varepsilon_{Nd}(t)$ are listed in Table 3.

4. Results

4.1. Zircon U–Pb geochronology

Sample 05SD-21 is a dolerite collected from the Yedian area, about 35 km northeast of Mengyin city (N35°52.298′, E118°07.171′). It comprises 40% clinopyroxene, 52% plagioclase and minor amphibole, biotite, quartz and chlorite. The most plagioclase grains are ~0.2–0.6 mm sized, and clinopyroxene grains are ~0.1–0.4 mm sized. Zircons separated from the sample are mostly euhedral in morphology, and transparent and light brown in color. The cathodoluminescence images show that these zircons have commonly concentric oscillatory zoning with low to variable luminescence (inset in Fig. 2a), an indicative of a magmatic origin. All 28 analyses give a wide range in U (65–979 ppm) and Th (84–951 ppm) concentration, and Th/U ratios are in range from 0.35 to 1.28 (Fig. 2a). These analyses constitute a well-defined regression line with the upper intercept age of 1841 ± 17 Ma (Fig. 2b). Of these analyses, spot 05SD-21-4 yielded a concordia age of 1853 ± 24 Ma, consistent with the upper intercept age. This age can be interpreted as the crystallization age of the dyke, indicating a Paleoproterozoic origin. The age is also consistent with the SHRIMP zircon age of 1837 ± 17 Ma obtained for the Taishan dyke (Hou et al., 2006).

4.2. Geochemical characteristics

The studied dykes display small variations in major oxide compositions, with $SiO_2 = 51.86$–53.83%

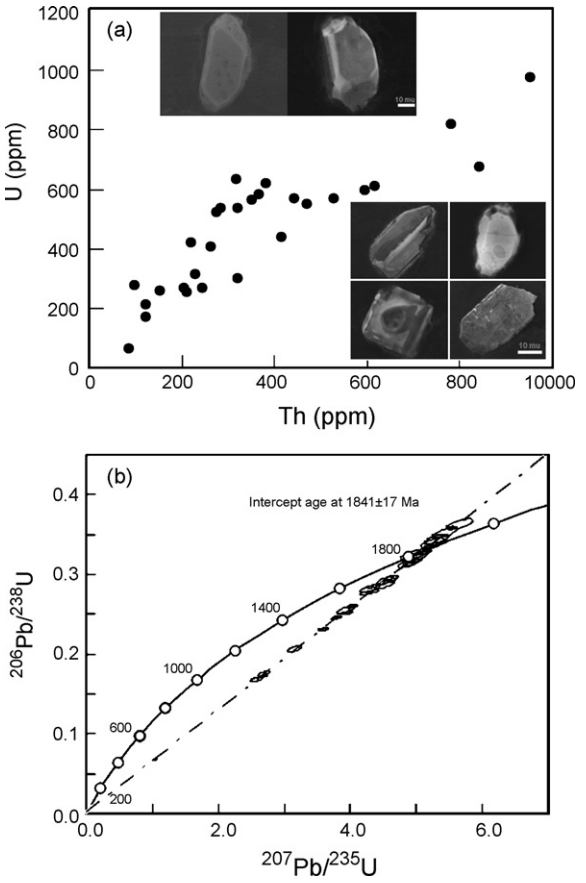

Fig. 2. (a) Zircon Th–U plot and (b) LA-ICP-MS U–Pb zircon concordia diagram for 05SD-21 diabasic dyke. Inset in (a) shows the CL image of representative zircon. Scale bar = 100 μm.

(volatile-free to 100%), MgO = 5.62–6.39%, Al_2O_3 = 12.9–13.9%, FeOt = 11.04–12.18% and TiO_2 = 2.02–2.24% (Table 2). They have K_2O of 1.36–2.30% and total alkalis ($Na_2O + K_2O$) of 3.63–5.52% with K_2O/Na_2O of 0.50–0.78. These dykes belong to the sub-alkaline basalts and basaltic andesites on the basis of the diagrams of major oxides (Fig. 3a) and Nb/Y versus Zr/Ti ratios (no shown). In the diagram of SiO_2 versus K_2O (Fig. 3b), these samples plot into the low- to medium-potassium fields. The *mg*-numbers (=Mg/(Mg + ΣFe) in atomic ratio) are in the range of 0.47–0.51. Cr and Ni contents vary from 184 to 225 ppm and 83 to 101 ppm, respectively. These samples have lower FeOt and higher Al_2O_3 contents relative to those of the MORB (Hawkins, 1995; Hickey-Vargas et al., 1995), but higher TiO_2 and FeOt and lower Al_2O_3 contents comparable to the Mariana and Okinawa back-arc basins basalts (BABB) at comparable MgO (Volpe et al., 1987; Gribble et al., 1996, 1998; Shinjo et al., 1999). Although these samples have a narrow variation in SiO_2, it is general that FeOt, CaO and TiO_2 correlate negatively with SiO_2 whereas Al_2O_3 and $K_2O + Na_2O$ correlate positively with SiO_2. The TiO_2 and P_2O_5 contents are slightly variable irrespective of Zr contents (Fig. 4a and b). As shown in Fig. 4c–l, Zr contents correlate negatively with compatible elements (e.g., Cr, Ni, V and Co) whereas correlate positively with incompatible elements (e.g., Th, La, Sr, Nb, Hf and Y).

These dykes have (La/Yb)cn = 8.97–11.36, (La/Sm)cn = 2.45–2.92 and (Gd/Yb)cn = 2.45–2.71, with Eu positive anomalies ($Eu/Eu^* = 1.06–1.26$). They have a similar REE pattern to those of arc-like volcanics and Seki basalts from the NE Japan, but have significantly higher LREE and lower HREE than those of N-MORB and E-MORB. In comparison with the BABB from the NE Japan, Western Eritrea, NW Hearne and Kuerti (Sandeman et al., 2006; Teklay, 2006; Shuto et al., 2006; Xu et al., 2003), these mafic dykes exhibit a stronger fractionation of LREEs relative to HREEs (Fig. 5a). On the primitive mantle-normalized spidergram (Fig. 5b), they are characterized by the subparallel spiky patterns

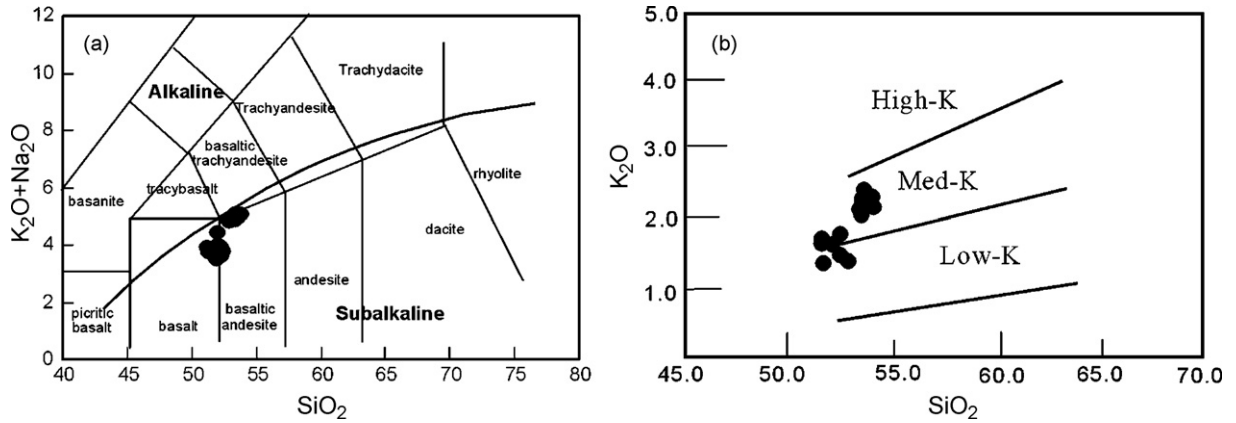

Fig. 3. (a) SiO_2 vs. $K_2O + Na_2O$ (after Middlemost, 1994) and (b) SiO_2 vs. K_2O (after Morrison, 1980) for the Paleoproterozoic mafic dykes in the Eastern Block, the NCC.

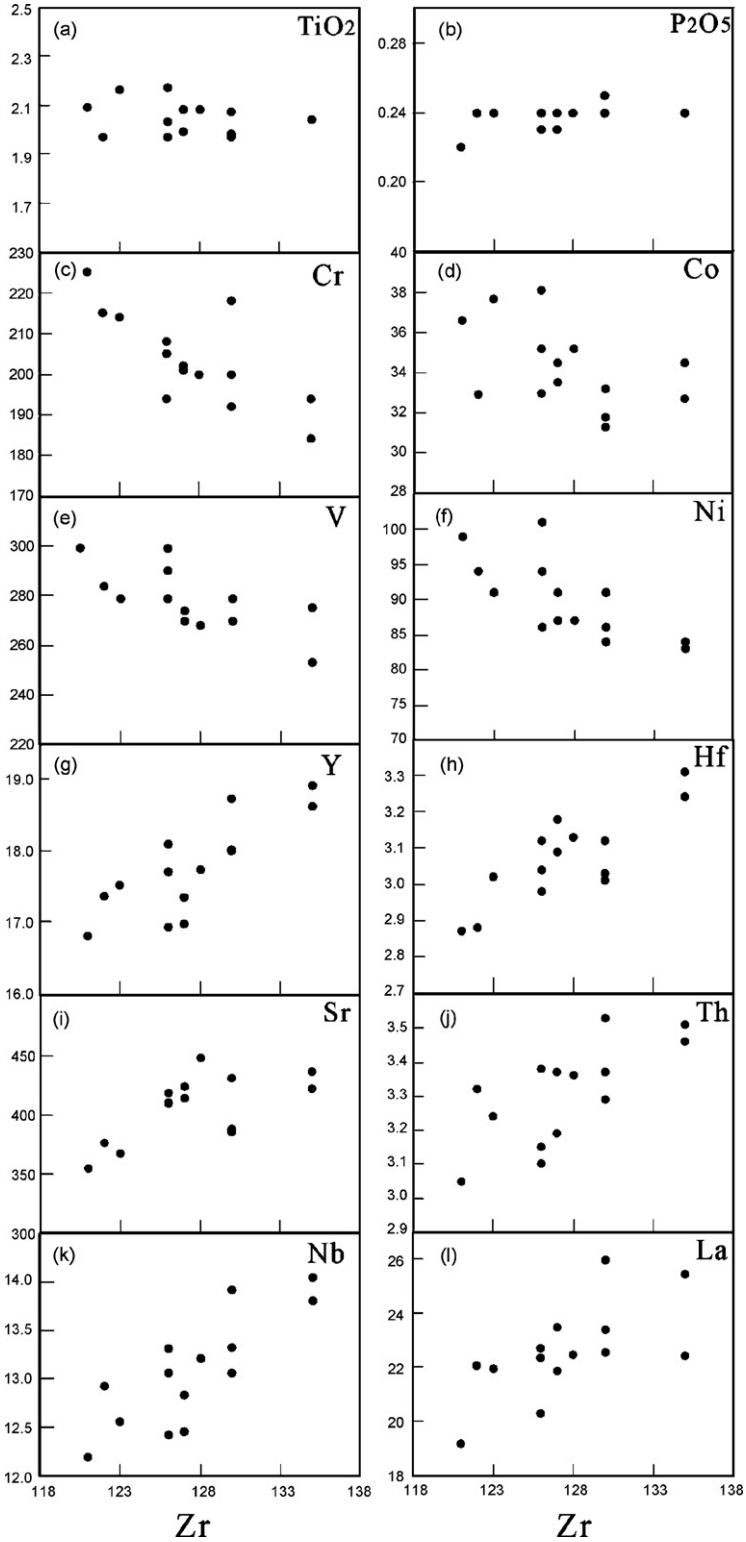

Fig. 4. Plots of Zr vs. (a) TiO_2, (b) P_2O_5, (c) Cr, (d) Co, (e) V, (f) Ni, (g) Y, (h) Hf, (i) Sr, (j) Th, (k) Nb, and (l) La for the Paleoproterozoic mafic dykes in the Eastern Block in the NCC.

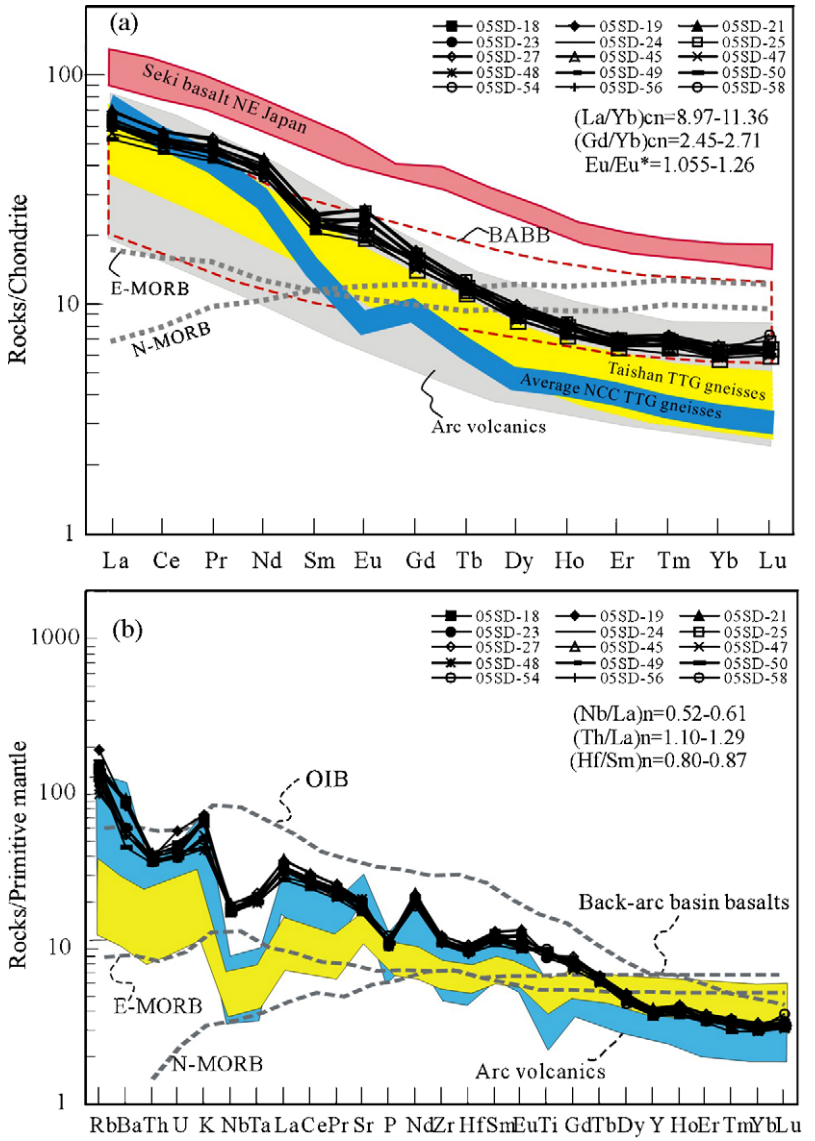

Fig. 5. (a) Chondrite normalized rare-earth element and (b) primitive mantle-normalized spidergram for the Paleoproterozoic mafic dykes in the Eastern Block in the NCC. Chondrite- and primitive mantle-normalize values are from Taylor and McLennan (1985), and Sun and McDonough (1989), respectively. Data for BABB are from Shinjo et al. (1999), Sandeman et al. (2006) and Teklay (2006). Seki basalts NE Japan are from Shuto et al. (2006). N-MORB and E-MORB are after Sun and McDonough (1989). Taishan TTG gneisses and average NCC TTG rocks are from Jahn et al. (1988) and Liu et al. (2004), respectively.

with enrichment in LILEs (e.g., Rb, Th and La) and depletion in HFSEs (e.g., Nb–Ta and Zr–Hf). $(Nb/La)_N$ and $(Hf/Sm)_N$ are in range of 0.52–0.61 and 0.80–0.87, respectively, exhibiting an elemental geochemical affinity to arc volcanic rocks. Negative P anomalies are also apparent. These dykes have lower Nb and Ta contents and higher Th/Nb, Th/Yb and La/Yb ratios than those of average MORB.

The initial Sr isotopic ratios vary from 0.702859 to 0.703706, and $\varepsilon_{Nd}(t)$ values range from +3.82 to +7.42 (Table 3). They plot into a relatively narrow range along the mantle array (Fig. 6). Such Sr–Nd isotopic compositions are stronger depleted relative to arc volcanic rocks, but slightly enriched comparable with the MORB source (e.g., Ohki et al., 1994; Shuto et al., 2006). These samples studied here exhibit similar initial Sr–Nd isotopic compositions to the BABB from the Proterozoic western Eritrea, Paleozoic Kuerti and middle-late Miocene NE Japan, (e.g., Teklay, 2006; Shuto et al., 2006; Xu et al., 2003). However, lower initial Sr isotopic

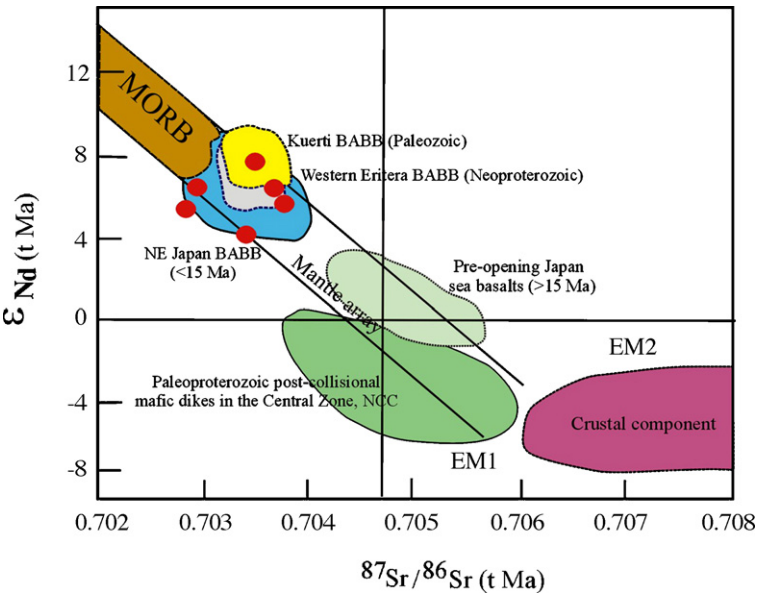

Fig. 6. Initial $^{87}Sr/^{86}Sr(t)$ versus $\varepsilon_{Nd}(t)$ ($t = 1850$ Ma) diagram for the Paleoproterozoic mafic dykes in the Eastern Block. The BABB fields for NE Japan (middle-late and early Miocene), western Eritrea (Neoproterozoic) and Kuerti (Paleozoic) are from Shuto et al. (2006), Teklay (2006) and Xu et al. (2003), respectively. The range of the age-comparable post-collisional mafic dykes for the TNCO is from Wang et al. (2004, in press).

ratios and higher $\varepsilon_{Nd}(t)$ values are shown compared to the age-comparable post-collisional TNCO mafic dykes (Wang et al., 2004, in press). $^{147}Sm/^{144}Nd$ ratios of these dykes range from 0.110 to 0.120, and T_{DM} values (time of removal from depleted mantle) are in range of 1.79–1.98 Ga.

5. Discussions

5.1. Magma process

As shown above, the studied samples have mg-number of 0.47–0.51, indicating that the magma might experience somewhat differentiation of olivine and pyroxene. This fractionation is also evidenced by a decrease in MgO and FeOt with an increase in SiO_2, and decreasing compatible elements (e.g., Cr, Co, V and Ni) contents with increasing Zr contents (Fig. 4c–f). Apatite and Fe–Ti oxides fractionations should be insignificant since TiO_2 and P_2O_5 contents among these samples are relatively constant irrespective of Zr (Fig. 4a and b) or SiO_2. Plagioclase fractionation may not have played an important role as suggested by slightly positive Eu anomalies (Fig. 5a). However, a crustal-like elemental systematics, as suggested by LILEs and LREEs enrichments and associated Nb–Ta and Zr–Hf depletions, cannot be explained only by the crystallization fractionation alone. The involvement of crustal components, either in source regions or crustal assimilation en route, is a most likely alternative.

On diagrams of Zr versus REE, HFSE, Ni and Cr (Fig. 4c–l), these samples generally display linear variations, indicative of a limited mobility of these elements during alteration. In order to better evaluate the source nature, it is vitally necessary, even difficult, to assess possible effects of crustal assimilation en route. Even assuming that a MORB-derived magma has $SiO_2 = 50$ wt%, Nd = 25 ppm, $(Nb/La)_N = 0.90$ and $\varepsilon_{Nd}(t) = 9.0$, and the average TTG rocks in the NCC (most likely the crustal contaminated component in the complex) has $SiO_2 = 66$ wt%, Nd = 35 ppm, $(Nb/La)_N = 0.10$ and $\varepsilon_{Nd}(t) = -8.0$, a simple mixing calculations show that the crustal assimilation should not be more than 20% in order to match with the observed SiO_2 and $\varepsilon_{Nd}(t)$ values. However, to match with the observed $(Nb/La)_N$ ratios of 0.52–0.61, at least 40–50% TTG rocks are required to be involved into the MORB-derived magma. Such high proportional crustal assimilation necessarily modifies the primary basaltic magma into intermediate-acid rocks, and thus is unrealistic.

The preceding T_{DM} values are similar to the crystallization age of the dykes, also indicating, within the resolution of the Nd isotopic system, that these samples were derived from a source insignificantly contaminated by older continental crust, also evidenced by the DM-like ε_{Nd} ($t = 1850$ Ma) values. As shown in Fig. 5a, the

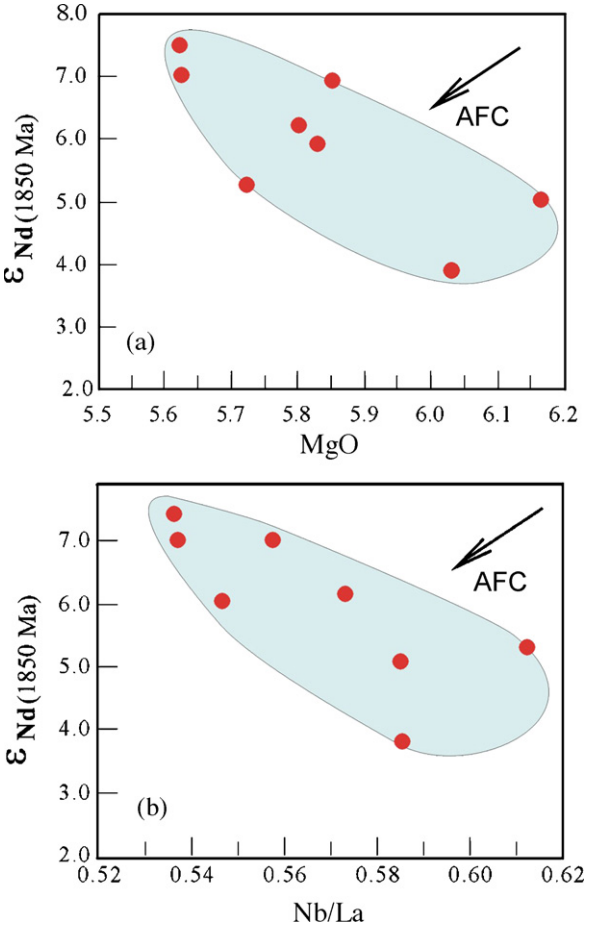

Fig. 7. Plots of (a) MgO vs. $\varepsilon_{Nd}(t)$, and (b) Nb/La vs. $\varepsilon_{Nd}(t)$ for the Paleoproterozoic mafic dykes in the Eastern Block, the NCC.

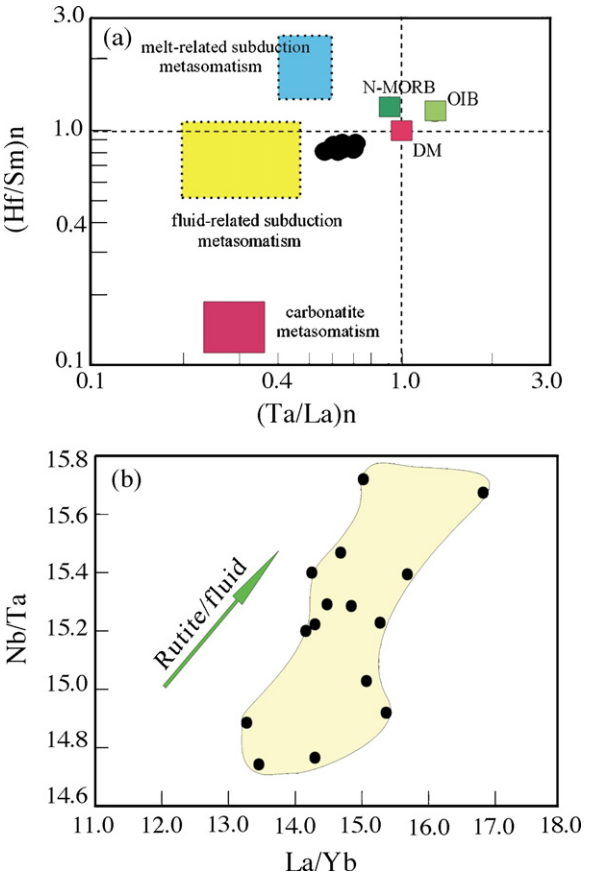

Fig. 8. (a) $(Ta/La)_N$ vs. $(Hf/Sm)_N$ and (b) Nb/Ta vs. La/Yb diagrams for the Paleoproterozoic mafic dykes in the Eastern Block, NCC. Original diagram of (a) is after LaFlèche et al. (1998) and the trend of the rutile/fluid in (b) is from Münker (1998).

samples have similar LREE but higher MREE contents relative to the average TTG rocks of the NCC (Liu et al., 2004). In comparison with the Taishan TTG gneisses, they have similar REE patterns but lower REE contents (Jahn et al., 1988; Fig. 5a). $(Th/Nb)_N$ ratios, which act as an indicator for the extent of crustal contamination, are in range of 2.02–2.20 for these samples, similar to that of E-MORB with $(Th/Nb)_N$ ratios of 2.0. Sample 05SD-21 with the highest $\varepsilon_{Nd}(t)$ value shows relatively lower *mg*-number and $(Nb/La)_N$ and higher SiO_2. Whereas, Sample 05SD-19 with the lowest $\varepsilon_{Nd}(t)$ value exhibits higher MgO and $(Nb/La)_N$ and lower SiO_2. In the plots of MgO, Nb/La and $\varepsilon_{Nd}(t)$ (Fig. 7a and b), negative correlations are generally shown, in contrary to those caused by crustal assimilation or assimilated fractionation process (DePaolo, 1981). In our study, the inherited zircon grains have not been observed in the sample 05SD-21 (Fig. 2b). Thus, these observations appear to more favor a scenario of insignificantly crustal assimilation in spite that the crustal contamination en route could not completely been excluded. As a result, the arc-like elemental geochemical signatures of these samples are more likely indicative of source nature.

5.2. Source nature of the magma

The observed Sr–Nd isotopic compositions for these dykes from western Shandong Complex display an affinity to a MORB source, but show an excursion trend towards crustal component along the mantle array (Fig. 6). MgO and TiO_2 contents for these dykes are similar to those MORB-derived magmas but are higher than those of arc volcanics. SiO_2, $A1_2O_3$ and Fe_2O_3 are lower than those of arc volcanics. In comparison with the MORB-derived magma, they are more enriched in LILEs and LREEs contents and variably depleted in Ti, Y, Yb and other HREE (Fig. 5a). In the $(Th/La)_N$ versus $(Hf/Sm)_N$ diagram (Fig. 8a), the data are plotted along

the trajectory between the MORB and arc component related to metasomatism of the subducted-fluids. The Ba/La and Ce/Pb ratios of these samples show a positive correlation with (La/Yb)cn, suggesting a mixing curve between MORB component (low Ba/La, Ce/Pb and low La/Yb) and possible arc component (high Ba/La, Ce/Pb and La/Yb). The arc-like elemental geochemical signatures for these mafic dykes, including an enrichment in LREEs, LILEs and a depletion in HFSEs as well as significant negative Nb–Ta, Zr–Hf and P anomalies, could be explained by the two possible petrogenetic models if significant crustal contamination through crust is not considered. One is inherited from the ancient lithospheric source and other is related to introduction of metasomatized melt/fluid released from the newly subducted slab.

In western Shandong Complex characterized by the Taishan greenstone belt, there is no evidence for subduction/collision during Neoarchean (∼2700 Ma) and Paleoproterozoic (∼1900 Ma) times (e.g., Cao et al., 1996; Zhao et al., 2005; Jahn et al., 1988; Polat et al., 2006). In contrast, a geodynamic model related to plume–craton interaction at ∼2700–2800 Ma is proposed (Zhao et al., 1998; Polat et al., 2006). The komatiites in the Taishan greenstone belt display a relatively large range of $\varepsilon_{Nd}(t = 2700\,Ma)$ values ranging from −0.4 to +3.6 (Polat et al., 2006), and the TTG rocks emplaced into the greenstone belt are characterized by $\varepsilon_{Nd}(t = 2700)$ values of +2.2 to +3.4 (Jahn et al., 1988). Such an Archaean lithospheric source beneath the Taishan area should have $\varepsilon_{Nd}(t = 1850)$ values of <+1 and an initial Sr isotopic ratio of >0.7045 when it evolved till Paleoproterozoic time (e.g., Jahn et al., 1988), which are distinct from the observed Sr–Nd isotopic compositions for these studied dykes. Even assuming that the analytical content on Sm is 110% of actual content whereas the analytical value on Nd is only 90% of actual content, the calculated $\varepsilon_{Nd}(t)$ values for these dykes are also in range of +1.37 to +4.80. Thus, such depleted Sr–Nd isotopic systematics for these dykes, even considering Sm and Nd analytical errors, might not be directly inherited from a Neoarchean lithospheric source with the involvement of a long resident "old" component. It is most likely that they shared a source region related to the dehydration and/or melting of newly subducted slab in convergent margin (e.g., McCulloch and Gamble, 1991; Pearce and Peate, 1995; Shinjo et al., 1999).

A further dispute remains as to whether or not such "crustal" signatures might originate from either dehydrated fluids or melts from a subducted slab. The depletion and differentiation of Nb and Ta are considered to be a result of the initial partitioning and subsequent equilibration between rutile and fluids or melts in a subducted slab (e.g., Münker, 1998). A negative correlation (high Nb/Ta-trend with Nb/Ta ratio of >17.6) and a positive correlation (low Nb/Ta-trends with Nb/Ta ratio of <17.6) between Nb/Ta and La/Yb (or Th/Yb) suggest that they may have been derived from the decomposition of rutile in melts and fluids, respectively (Münker, 1998). These samples have Nb/Ta ratios of 14.7–15.7 (Table 2) and exhibit an increase in Nb/Ta with increasing La/Yb (Fig. 8b). Depletions of Ta and Hf relative to La and Sm, respectively, are commonly considered to result from the fluid-related metasomatism via a subduction process (LaFlèche et al., 1998). $(Ta/La)_N$ ratios range from 0.57 to 0.72 and $(Hf/Sm)_N$ from 0.80 to 0.87 for these samples (Table 2), and plot closer to the field of the subduction-related fluids rather than melt-related metasomatism (Fig. 8a). The slightly variable Nb/Y and Nb/Zr relative to Ba/Y and Th/Zr, respectively, are also consistent with an increasing fluid-related metasomatism in the source (e.g., Kepezhinskas et al., 1997). Therefore, the dykes exhibit a geochemical affinity to both arc volcanics and MORB source, and most likely originated from a MORB-like source metasomatized by newly subduction-related fluids potentially via source contamination through a subduction process.

5.3. An intra-continental back-arc basin

As shown in Fig. 5a, the REE pattern of these samples is almost identical to that of early Miocene Seki basaltic rocks, which is interpreted as products of the pre-Japan Sea opening (Shuto et al., 2006). It is also similar to that of the basaltic rocks found in Rio Grande continental rift (Leat et al., 1990). On the basis of the elemental systematics, Hou et al. (2005) interpreted the mafic dikes as having formed under an intra-continental rift environment. However, the mafic rocks from the intra-continental rifting, especially in the Archaean lithospheric mantle, should have lower initial epsilon values, distinct from the observed isotopic composition of these studied dykes. In order to match with such high $\varepsilon_{Nd}(t)$ values for these dykes, the proportion should be less than 5% for the involvement of lithospheric component into the asthenospheric source even considering asthenosphere–lithosphere interaction. Such lower degree addition of the lithospheric component could not reasonably explain the arc-like elemental systematics for these dykes. Thus the decouple between higher $\varepsilon_{Nd}(t)$ values and greater abundances of LILE and higher LILE/HFSE ratios might also not result from a physical mixing of arc- and MORB-type mantle.

Two tectonic setting, including fore-arc and back-arc basins, could be put forward to explain the elemental and isotopic systematics for these dykes. It is usual that volcanic rocks from a fore-arc basin have a wide range of major oxides and compound rock-associations varying from boninitic and high-mg andesitic to felsic components, as observed in the Isu–Bonin fore-arc basin (e.g., Wallin and Metcalfe, 1998). However, this possibility is not supported due to the relatively uniform major oxides composition for these dykes and absence of contemporaneous volcanics in the Eastern Block. Moreover, available data suggest that the western margin of the Eastern Block faced a major ocean, which eastwardly subducted beneath the western margin of the Eastern Block during Neoarchean–Paleoproterozoic time (e.g., Zhao et al., 2005 and reference therein). An alterative is a back-arc basin regime for the geochemical characteristics of MORB- and arc-like end-members, as suggested by the BABB from the northern Mariana, middle-late Miocene NE Japan, Proterozoic western Eriterea and Heimefrontfjella (East Antarctica), and Neoarchean NW Hearne (e.g., Volpe et al., 1987; Stern et al., 1990; Pouclet et al., 1995; Hawkins, 1995; Hickey-Vargas et al., 1995; Gribble et al., 1996, 1998; Shinjo et al., 1999; Bauer et al., 2003; Shuto et al., 2006; Teklay, 2006; Sandeman et al., 2006).

In the FeO^*/MgO versus TiO_2 diagram (Fig. 9a), these samples plot into the field of BABB (Miyashita et al., 1995; Shuto et al., 2006). Na8 and Fe8 contents fractionation-corrected to a common 8% MgO by Na_2O and FeO contents, respectively, exhibit an affinity to both MORB-like and arc-like compositions (Fig. 9b), and overlap into the ranges of the Lau, Manus, Mariana and east Scotia BABB (Taylor and Martinez, 2003). Ce/Pb = 6.2–13.1 and Ba/La = 16.6–28.9 for these dykes are similar to those of the Northern Okinawa BABB

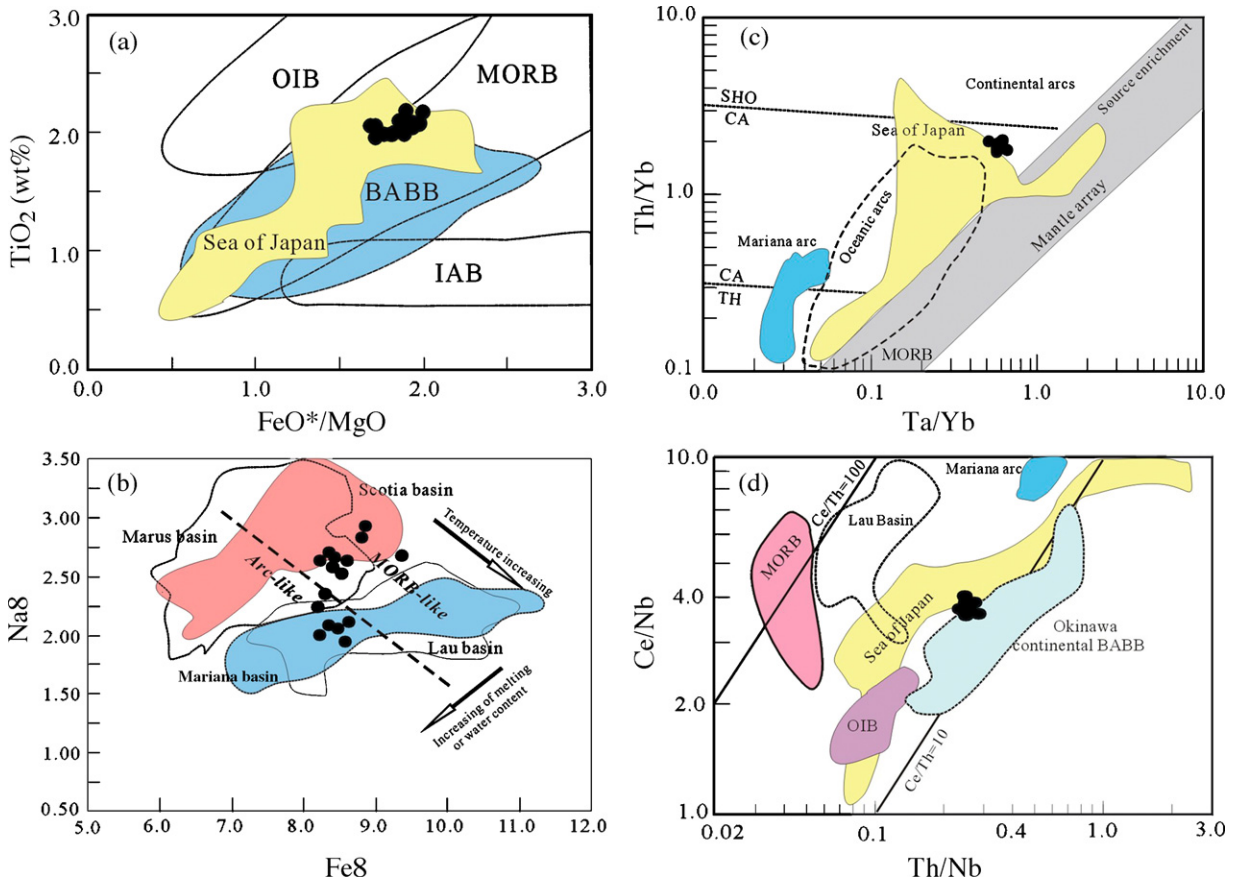

Fig. 9. Plots of (a) FeO^*/MgO vs. TiO_2 (after Shuto et al., 2006), (b) Fe8 vs. Na6 (after Taylor and Martinez, 2003), (c) Th/Yb vs. Ta/Yb (after Pearce and Peate, 1995), and (d) Ce/Nb vs. Th/Nb (after Sandeman et al., 2006) for the Paleoproterozoic mafic dykes in the Eastern Block. Fields of the BABB and Sea of Japan are by Miyashita et al. (1995) and Shuto et al. (2006). In (b), Sea of Japan, Mariana arc, Lau Basin and Okinawa BABB are from Pouclet et al. (1995), Pearce and Peate (1995) and Shinjo et al. (1999). $Na8 = [Na_2O + 0.115(8\text{-MgO})]/[1 + 0.133(8\text{-MgO})]$ (Plank and Langmuir, 1992), and $Fe8 = [FeO^* + 8\text{-MgO}]/[1 + 0.25\ (8\text{-MgO})]$, where FeO^* is total Fe contents (Taylor and Martinez, 2003).

(Shinjo et al., 1999). All samples plot above the mantle array in the Th–Ta–Yb diagram (Fig. 9c), having Ta/Yb and Th/Yb ratios close to continental arc volcanics. On the Th/Yb versus Ta/Yb, Th/Nb versus Ce/Nb and Th/Nb versus (La/Sm)n diagrams (Fig. 9c and d), the elevated Th/Yb and Th/Nb are also plotted into the field of the Japan Sea BABB (e.g., Pouclet et al., 1995; Sandeman et al., 2006). Similar consideration is also monitored on some of plots of HFSE and REE ratios.

Questions remain as to whether the Paleoproterozoic back-arc basin developed on an intra-oceanic lithosphere or a continental basement. The elevated LILEs, LREEs and HFSEs, relatively low (Th/La) and slightly enriched isotopic compositions are comparable to those observed in the continental BABB (Gribble et al., 1998; Sandeman et al., 2006). Zr/Y ratios for these samples are in range of 6.9–7.5, overlapped those of continental arc basalts. In the Y/15–La/10–Nb/8 plot (on shown), they plot into the field of continental basalt nearer to that of volcanic arcs relative to continental rifts. A similar conclusion is also revealed in the TiO_2–K_2O–P_2O_5 discriminant plot, which is an effective means of discriminating environments of the oceanic and non-oceanic basalts (Pearce et al., 1975). The incompatible elemental ratios (e.g., Th/Yb, Ta/Yb and Th/Nb) for these dykes are closer to those of the intra-continental Middle Okinawa BABB rather than intra-oceanic Mariana BABB (Fig. 9c and d; e.g., Volpe et al., 1987; Gribble et al., 1998; Shinjo et al., 1999). Additionally, it is common that the intra-oceanic BABB from the western Pacific are geochemically indistinguishable from a N-MORB source (e.g., Hickey-Vargas et al., 1995; Hawkins, 1995) and have (La/Yb)n < 2, Nb/La > 0.5, Ba/La < 10 and Sm/Nd > 0.3. By contrast, the BABB with continental basement from western Pacific usually exhibit E-MORB or OIB-like elemental and isotopic composition with (La/Yb)n > 3, Nb/La > 0.6, Ba/La > 10 and Sm/Nd < 0.3 (e.g., Hickey-Vargas et al., 1995; Shinjo et al., 1999). All samples analyzed here have (La/Yb)n = 39.0–11.4, Ba/La = 16.6–28.9, Nb/La = 0.55–0.64 and Sm/Nd = 0.18–0.21, closer to those of the intra-continental BABB from western Pacific. Here we infer that the MORB component is from the upwelling asthenosphere. The strong arc-type elemental signature for these dykes is inherited from the continental arc-rifting related to the early evolutionary of back-arc spreading, similar to those of the Bransfield Strait and Sumisu Rift back-arc basin systems (e.g., Weaver et al., 1979; Stern et al., 1990). The crust that formed just after arc rifting has a stronger arc affinity compared to that forming later as the back-arc basin widened and matured. Consequently, the preceding compositional signatures and interpretations for these dykes more likely suggest an intra-continental back-arc basin regime, analog to the modern Okinawa back-arc basin (Shinjo et al., 1999). These dykes might represent the remnants of a Paleoproterozoic extensional or failed back-arc basin system developed in the Eastern Block of the NCC. Although the age-similar, arc-related volcanics on the Shandong Complex have not yet been identified, we cannot preclude the existence of such rocks since extensive mapping work has not been carried out in the region (Cao et al., 1996). Our recent investigation has showed that some unmetamorphosed Paleoproterozoic dykes in the region are characterized by LILE-enrichment, HFSE-depletion and initial epsilon <-2.0 (authors' unpublished data), geochemically similar to those arc volcanics. Additionally, the possible Paleoproterozoic arcs volcanics might be denudated and eroded during Paleo- and Meso-Proterozoic times due to the contemporaneous uplift of >3 km in the NCC (e.g., Wang et al., 2003). Here we also accept such a suspensive consideration, and work to resolve this issue is still on going.

5.4. Tectonic implications

Two distinct hypotheses have been postulated for the 1.85 Ga tectonothermal event that happened in the NCC (e.g., Wilde et al., 2002; Zhao et al., 1999, 2000, 2001, 2002a,b, 2003, 2005; Kusky and Li, 2003; Zhai and Liu, 2003; Wang et al., 2003, 2004). One school of thought interprets it as an intra-continental extension event related to a mantle plume (e.g., Zhai and Liu, 2003; Kusky and Li, 2003; Hou et al., 2006), whereas others consider it as a continental collisional event (Fig. 1a; e.g., Zhao et al., 1999, 2000, 2001, 2003, 2005; Liu et al., 2002, 2005, 2006; Guo et al., 2002; Wang et al., 2003, 2004; Kröner et al., 2005, 2006; Wilde et al., 2002; Wilde and Zhao, 2005).

In the mantle plume-related hypothesis, mafic dykes in the TNCO and Eastern Block are considered to have been simultaneously emplaced in a plume-driven extensional setting. However, the available data show that the unmetamorphosed mafic dykes in the TNCO were emplaced in the period of 1781–1765 Ma (Halls et al., 2000; Peng et al., 2005; Wang et al., 2004), later than the main time of the Paleoproterozoic thrusting, metamorphism and crustal upwelling in the TNCO (Wang et al., 2003; Zhao et al., 1999, 2001, 2002a,b, 2003, 2005 and references therein). In contrast, the mafic dykes in the Eastern Block have crystallization ages of 1837–1841 Ma, synchronously with the major thrusting

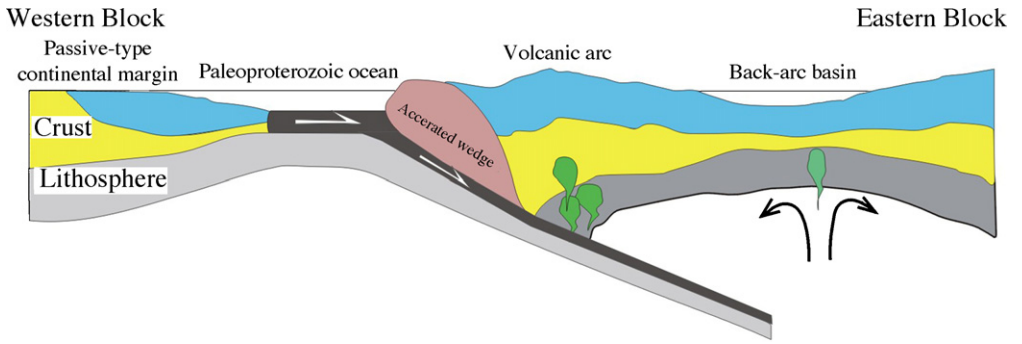

Fig. 10. A schematic cartoon showing the development of the Paleoproterozoic back-arc basin in the continental hinterland of the Eastern Block.

and metamorphic event in the TNCO. Nearly all mafic dykes in the TNCO are characterized by an enrichment in LILEs, a depletion in HFSEs and low $\varepsilon_{Nd}(t)$ values of mainly −2.5 to −5.5, distinct from those of a mantle plume (Wang et al., 2004, in press). The synchronous volcanics from the Xiong'er Group at the southern margin of the NCC composed of andesites, dacites and rhyolites with minor basaltic andesites and sediment interlayers and exhibit low $\varepsilon_{Nd}(t)$ values of −2 to −9 (Zhao et al., 2002a,b), inconsistent with typical magmatic assemblages derived from mantle plumes. The mafic dykes in the Eastern Block exhibit prominent negative HFSE (arc-like) anomalies and MORB-like isotopic compositions, also distinct those magmatic assemblages from mantle plumes. In contrast, their isotopic signatures more support a source contamination of subducted components, which was likely added to the sub-arc mantle immediately prior to or during magmatism. Therefore, the emplacement of mafic dykes in both the TNCO and the Eastern Blocks may not have been related to a mantle plume event; they were most probably related to the subduction and subsequent collision between the Eastern and Western Blocks. Followed by the process of subduction/collision, the asthenosphere upwelling at the continental margin far away the suture occurred, accompanied by the involvement of the subduction-derived fluid and rifting in the crust, resulting in the production of the intra-continental back-arc basin magmas with the Eastern Block.

There is still no consensus on the timing of the collision between the Western and Eastern Block. Some researchers believe that it occurred at ∼2.5 Ga (e.g., Kusky et al., 2001; Kusky and Li, 2003) whereas others consider that the two blocks were finally amalgamated at ∼1.85 Ga (e.g., Wilde et al., 1998, 2002; Wilde and Zhao, 2005; Kröner et al., 2005, 2006; Liu et al., 2006; Zhao et al., 1999, 2000, 2001, 2002a,b, 2005 and reference therein). The presence of Paleoproterozoic mafic dykes that developed in an intra-continental back-arc basin at the western margin of the Eastern Block supports Paleoproterozoic collision model for the NCC. Other lines of evidence supporting the Paleoproterozoic collision model include that: (1) only one generation of 1870–1820 Ma metamorphic zircons was identified in the metamorphic rocks of the TNCO (e.g., Zhao et al., 1999, 2000, 2001, 2002a,b, 2003, 2005); (2) increasing, metamorphism for the Wutai and Lüliang Complexes revealed by monazite dating occurred in 1880–1822 Ma (Liu et al., 2006); (3) a collision-thrusting/thickening-extensional collapse cycle reconstructed by Wang et al. (2003) have happened between ∼1870 and ∼1790 Ma. Considering clockwise P–T paths of metamorphic rocks in the TNCO, we advocate that the western margin of the Eastern Block faced a major ocean during Neoarchean to early Paleoproterozoic times, which underwent eastward subduction beneath the western margin of the Eastern Block, along which some back-arc basins were developed in the continental hinterland in response to upwelling asthenosphere, as shown in Fig. 10. Accompanied with the decompression melting of the upwelling asthenospheric mantle, the fluids from the subducted slab carried the "crustal" signatures into the overlying mantle and cause the partial melting of the newly metasomatized source to generate the Paleoproterozoic mafic dykes in the Eastern Block. This is supported by geochemical data of these dikes, which suggest that the western margin of the Eastern Block during Paleoproterozoic time resemble those back-arc basins that develop along the western Pacific Ocean.

Acknowledgements

The authors would like to thank X.-Y. Chen and J.-W. Zhi for important assistance in preparing samples. We also thank two anonymous reviewers for their thorough, critical and constructive reviews and comments, and P.A.

Cawood for his helpful editorial advice. Financial support is provided by Hong Kong RGC Projects (7055/03P, 7058/04P, 7055/05P and 7063/06P); the Nature Sciences Foundation of China (40303005, 40473019 and 40334039) and GIG (CAS) grant (GIGIso-06-03).

References

Bauer, W., Jacobs, J., Fanning, C.M., Schmidt, R., 2003. Late Mesoproterozoic Arc and Back-arc Volcanism in the Heimefrontfjella (East Antarctica) and Implications for the Palaeogeography at the Southeastern Margin of the Kaapvaal-Grunehogna Craton. Gondwana Res. 6 (3), 449–465.

Cao, G., Wang, Z., Cheng, Z., Dong, Y., Li, P., Wang, S., Jin, L., Shen, K., Xu, J., Shen, K., Shi, Y., Xu, H., Zhan, C., Zheng, L., Zhang, Z., Ren, X., Zai, Y., Ma, Y., Liang, B., 1996. Early Precambrian Geology of Western Shandong. Geological Publishing House, Beijing, pp. 1–210 (in Chinese with English Abstract).

DePaolo, D.J., 1981. Trace element and isotopic effects of combined wall rock assimilation and fractional crystallization. Earth Planet. Sci. Lett. 53, 189–202.

Gribble, R.F., Stern, R.J., Bloomer, S.H., Stuben, D., O'Hearn, T., Newman, S., 1996. MORB mantle and subduction components interact to generate basalts in the southern Mariana Trough back-arc basin. Geochim. Cosmochim. Acta 60, 2153–2166.

Gribble, R.F., Stern, R.J., Newman, S., Bloomer, S.H., O'Hearn, T., 1998. Chemical and isotopic composition of lavas from the Northern Mariana Trough: implications for magmagenesis in back-arc-arc basins. J. Petrol. 39, 125–154.

Guo, J.H., O'Brien, P.J., Zhai, M.G., 2002. High-pressure granulites in the Sangan area, North China Craton: metamorphic evolution, P–T paths and geotectonic significance. J. Metamorph. Geol. 20, 741–756.

Halls, H.C., Li, J.H., Davis, D., Hou, G.T., 2000. A precisely dating Proterozoic palaeomagnetic pole from the North China craton and its relevance to palaeocontinental reconstruction. Geophys. J. Int. 143, 185–203.

Hawkins, J.W., 1995. The geology of the Lau Basin. In: Taylor, B. (Ed.), Back-arc Basins: Tectonics and Magmatism. Plenum Press, New York, pp. 63–138.

Hickey-Vargas, R., Hergt, J.M., Spadea, P., 1995. The Indian Ocean-type isotopic signatures in western Pacific marginal basins: origin and signatures. In: Taylor, B., Natland, J. (Eds.), Active Margins and Marginal Basins of the Western Pacific, Geophys. Monogr. Washington, DC, Ser. 88, pp. 175–197.

Hou, G.T., Liu, Y.L., Li, J.H., 2006. Evidence for ~1.8 Ga extension of the Eastern Block of the North China Craton from SHRIMP U–Pb dating of mafic dyke swarms in Shandong Province. J. Asian Earth Sci. 27 (4), 392–401.

Hou, G.T., Liu, Y.L., Li, J.H., Jin, A.W., 2005. The SHRIMP U–Pb chronology of mafic dyke swarms: a case study of Laiwu diabase dykes in western Shandong. Acta Petrologica et Mineralogica 24 (3), 179–185.

Jahn, B.M., Auray, B., Shen, Q.H., Liu, D.Y., Zhang, Z.Q., Dong, Y.J., Ye, X.J., Zhang, Q.Z., Cornichet, J., Mace, J., 1988. Archean crustal evolution in China: the Taishan Complex, and evidence for juvenile crustal addition from long-term depleted mantle. Precam. Res. 38, 381–403.

Jahn, B.M., Zhang, Z.Q., 1984. Archean granulite gneisses from eastern Hebei Province, China: rare earth geochemistry and tectonic implications. Contrib. Mineral. Petrol. 85, 224–243.

Kepezhinskas, P., McDermott, F., Defant, M.J., Hochstaedter, A., Drummond, M.S., 1997. Trace element and Sr–Nd–Pb isotopic constraints on a three-component model of Kamchatka Arc petrogenesis. Geochim. Cosmochim. Acta 61 (3), 577–600.

Kröner, A., Cui, W.Y., Wang, W.Y., Wang, C.Q., Nemchin, A.A., 1998. Single zircon ages from high-grade rocks of the Jianping Complex, Liaoning Province, NE China. J. Asian Earth Sci. 16, 519–532.

Kröner, A., Wilde, S.A., Zhao, G.C., O'Brien, P.J., Sun, M., Liu, D.Y., Wan, Y.S., Liu, S.W., Guo, J.H., 2006. Zircon geochronology and metamorphic evolution of mafic dykes in the Hengshan Complex of northern China: evidence for late Palaeoproterozoic extension and subsequent high-pressure metamorphism in the North China Craton. Precam. Res. 146 (1/2), 45–67.

Kröner, A., Wilde, S.A., Li, J.H., Wang, K.Y., 2005. Age and evolution of a late Archaean to early Paleozoic upper to lower crustal section in the Wutaishan/Hengshan/Fuping terrain of northern China. J. Asian Earth Sci. 24 (5), 577–595.

Kusky, T.M., Li, J.H., 2003. Paleoproterozoic tectonic evolution of the North China Craton. J. Asian Earth Sci. 22, 383–397.

Kusky, T.M., Li, J.H., Tucker, R.D., 2001. The Archean Dongwanzi ophiolite complex, North China Craton: 2.505-billion-year-old oceanic crust and mantle. Science 292, 1142–1145.

LaFlèche, M.R., Camire, G., Jenner, G.A., 1998. Geochemistry of post-Acadian, Carboniferous continental intraplate basalts from the Maritimes Basin, Magdalen islands, Quebec, Canada. Chem. Geol. 148, 115–136.

Leat, P.T., Thompson, R.N., Morrison, M.A., Hendry, G.L., 1990. Dickin Geochemistry of mafic lavas in the early Rio Grande Rift, Yarmony Mountain, Colorado, USA. Chem. Geol. 81, 23–43.

Liu, D.Y., Nutman, A.P., Compston, W., Wu, J.S., Shen, Q.H., 1992. Remnants of 3800 crust in the Chinese Part of the Sino-Korean craton. Geology 20, 339–342.

Liu, S.W., Pan, Y.M., Li, J.H., Li, Q.G., Zhang, J., 2002. Geological and isotopic geochemical constraints on the evolution of the Fuping Complex, North China Craton. Precam. Res. 117, 41–56.

Liu, S.W., Pan, Y.M., Xie, Q.L., Zhang, J., Li, Q.G., 2004. Archean geodynamics in the Central Zone. North China craton: constraints from geochemistry of two contrasting series of granitoids in the Fuping and Wutaishan complexes. Precam. Res. 130, 229–249.

Liu, S.W., Pan, Y.M., Xie, Q.L., Zhang, J., Li, Q.G., Yang, B., 2005. Geochemistry of the Paleoproterozoic Nanying Granitoid Gneisses: constraints on the tectonic setting of the Central Zone, North China Craton. J. Asian Earth Sci. 24 (5), 643–658.

Liu, S.W., Zhao, G.C., Wilde, S.A., Shu, G.M., Sun, M., Li, Q.G., Tian, W., Zhang, J., 2006. Th–U–Pb monazite geochronology of the Lüliang and Wutai Complexes: constraints on the tectonothermal evolution of the Trans-North China Orogen. Precam. Res. 148 (3/4), 205–224.

Liu, Y., Liu, H.C., Li, X.H., 1996. Simultaneous and precise determination of 40 trace elements in rock samples using ICP-MS. Geochimica 25 (6), 552–558.

Ludwig, K.R., 2001. Using Isoplot/EX. In: A Geochronological Toolkit for Microsoft Excel, version 2.49. Berkeley Geochronological Center, Berkeley, pp. 1-55, Spec. Publ.

McCulloch, M.T., Gamble, J.A., 1991. Geochemical and geodynamical constrains on subduction zone magmatism. Earth Planet. Sci. Lett. 102, 358–374.

Middlemost, E.A.K., 1994. Naming materials in the magma/igneous rock system. Earth Sci. Rev. 37, 215–224.

Miyashita, S., Tsuchiya, N., Ikeda, Y., Sakamoto, I., 1995. Petrology of the Okushiri Ridge Basalts in the Japan Sea Basin: arc- and plume-type magma series. Mem. Geol. Soc. Jpn. 44, 1–21.

Morrison, G.W., 1980. Characteristics and tectonic setting of the shoshonite rock association. Lithos 13, 97–108.

Münker, C., 1998. Nb/Ta fraction in a Cambrin arc-back system, New Zealand: source constraints and application of refined ICPMS techniques. Chem. Geol. 144, 23–45.

Ohki, J., Shuto, K., Kagami, H., 1994. Middle Miocene bimodal volcanism by asthenospheric upwelling: Sr and Nd isotopic evidence from the back-arc region of the Northeast Japan arc. Geochem. J. 28, 473–487.

Pearce, J.A., Gorman, B.E., Birkett, T.C., 1975. The TiO_2–K_2O–P_2O_5 diagram: a method of discriminating between oceanic and non-oceanic basalts. Earth Planet. Sci. Lett. 24, 419–426.

Pearce, J.M., Peate, D.W., 1995. Tectonic implications of the composition of volcanic arc magmatism. Annu. Rev. Earth Planet. Sci. 23, 251–285.

Peng, P., Zhai, M.G., Zhang, H.F., Guo, J.H., 2005. Geochronological constraints on the Paleoproterozoic evolution of the North China Craton: SHRIMP zircon ages of different types of mafic dykes. Int. Geol. Rev. 47 (5), 492–508.

Plank, T., Langmuir, C.H., 1992. Effects of the melting regime on the composition of the oceanic crust. J. Geophys. Res. 97, 19749–19770.

Polat, A., Li, J., Fryer, B., Kusky, T., Gagnon, J., Zhang, S., 2006. Geochemical characteristics of the Neoarchean (2800–2700 Ma) Taishan greenstone belt, North China Craton: evidence for plume–craton interaction. Chem. Geol. 230 (1/2), 60–87.

Pouclet, A., Lee, J.-S., Vidal, P., Cousens, B., Bellon, H., 1995. Cretaceous to Cenozoic volcanism in South Korea and in the Sea of Japan: magmatic constraints on the opening of the back-arc basin. In: Smellie, J.L. (Ed.), Volcanism Associated with Extension at Consuming Plate Margins. Geol. Soc. Spe. Pub. Lon., pp. 169–191.

Qian, X.L., Chen, Y.P., 1987. Late Precambrian mafic dyke swarms of the North China Craton. In: Halls, H.C., Fahrig, W.F. (Eds.), Mafic Dyke Swarms, Geol. Asso. Canada Spe. Paper 34, pp. 385–392.

Sandeman, H.A., Hanmer, S., Tella, S., Armitage, A.A., Davis, W.J., Ryand, J.J., 2006. Petrogenesis of Neoarchaean volcanic rocks of the MacQuoid supracrustal belt: a back-arc setting for the northwestern Hearne subdomain, western Churchill Province, Canada. Precam. Res. 144 (1/2), 126–139.

SDBGMR (Bureau of Geology and Mineral Resources of Shandong Province), 1991. Regional geology of Shandong Province. Geol Pub House, Beijing, pp. 1–441 (in Chinese).

Shinjo, R., Chung, S.L., Kato, Y., Kimura, M., 1999. Geochemical and Sr–Nd isotopic characteristics of volcanic rocks from the Okinwa Trough and Ryukyu Arc: implications for the evolution of a young, intracontinental back arc basin. J. Geophys. Res. 104 (B5), 10591–10608.

Shuto, K., Ishimoto, H., Hirahara, Y., Sato, M., Matsui, K., Fujibayashi, N., Takazawa, E., Yabuki, K., Sekine, M., Kato, M., Rezanov, A.I., 2006. Geochemical secular variation of magma source during Early to Middle Miocene time in the Niigata area, NE Japan: asthenospheric mantle upwelling during back-arc basin opening. Lithos 86, 1–33.

Stern, R.J., Lin, P., Morris, J.D., Jackson, M.C., Fryer, P., Bloomer, S.H., Ito, E., 1990. Enriched back-arc basin basalt from the northern Mariana Trough: implications for the magmatic evolution of back-arc basins. Earth Planet. Sci. Lett. 100, 210–225.

Sun, S.S., McDonough, W.F., 1989. Chemical and isotopic systematics of oceanic basalts: implication for mantle composition and processes. In: Sauders, A.D., Norry, M.J. (eds). Magmatism in the Ocean Basins. Geol. Soc. (London) Spe. Publ. 42, pp. 313–345.

Taylor, B., Martinez, F., 2003. Back-arc basin basalt systematics. Earth Planet. Sci. Lett. 210, 481–497.

Taylor, S.R., McLennan, S.M., 1985. The Continental Crust: Its Composition and Evolution. Oxford Press Blackwell, pp. 1–312.

Teklay, M., 2006. Neoproterozoic arc-back-arc system analog to modern arc-back-arc systems: evidence from tholeiite–boninite association, serpentinite mudflows and across-arc geochemical trends in Eritrea, southern Arabian-Nubian shield. Precam. Res. 145 (1/2), 81–92.

Volpe, A.M., Macdougall, J.D., Hawkins, J.W., 1987. Mariana Trough basalts (MTB): trace element and Sr–Nd isotopic evidence for mixing between MORB-like and Arc-like melts. Earth Planet. Sci. Lett. 82, 241–254.

Wallin, E.T., Metcalfe, R.V., 1998. Supra-subduction zone ophiolite formed in an extensional forearc: Trinity Terrane, Klamath Mountains, California. J. Geol. 106, 591–608.

Wang, Y.J., Fan, W.M., Zhang, Y.H., 2004. Geochemical, $^{40}Ar/^{39}Ar$ geochronological and Sr–Nd isotopic constraints on the origin of Paleoproterozoic mafic dykes from the southern Taihang Mountains and implications for the ca. 1800 Ma event of the North China Craton. Precam. Res. 135 (1/2), 55–79.

Wang, Y.J., Fan, W.M., Zhang, Y.H., Guo, F., 2003. Structural evolution and $^{40}Ar/^{39}Ar$ dating of the Zanhuang metamorphic domain in the North China Craton: constraints on Paleoproterozoic tectonothermal overprinting. Precam. Res. 122 (1–4), 159–182.

Wang, Y.J., Zhao, G.C., Fan, W.M., Peng, T.P., Sun, L.H., in press. Geochemistry of Paleoproterozoic (∼1770 Ma) mafic dykes from the Trans-North China Orogen and tectonic implications. J. Asian Earth Sci.

Weaver, S.D., Saunders, A.D., Pankhurst, R.J., Tarney, J., 1979. A geochemical study of magmatism associated with the initial stages of back-arc spreading. Contrib. Mineral. Petrol. 68, 151–169.

Wei, G.J., Liang, X.R., Li, X.H., Liu, Y., 2002. Precise measurement of Sr isotopic compositions of liquid and solid base using (LP) MC-ICP-MS. Geochimica 31 (3), 295–305.

Wilde, S.A., Cawood, P., Wang, K.Y., Nemchin, A., 1998. SHRIMP U–Pb zircon dating of granites and gneisses in the Taihangshan-Wutaishan area: implications for the timing of crustal growth in the North China Craton. Chin. Sci. Bull. 43 (144) (abstract).

Wilde, S.A., Zhao, G.C., 2005. Archean to Paleoproterozoic evolution of the North China Craton. J. Asian Earth Sci. 24 (5), 519–522.

Wilde, S.A., Zhao, G.C., Sun, M., 2002. Development of the North China Craton during the late Archean and its amalgamation along a major 1.8 Ga collision zone: including speculations on its position within a global Paleoproterozoic supercontinent. Gondwana Res. 5, 85–94.

Xia, X.P., Sun, M., Zhao, G.C., Li, H.M., Zhou, M.F., 2004. Spot zircon U–Pb isotope analysis by ICP-MS coupled with a frequency quintupled (213 nm) Nd-YAG laser system. Geochem. J. 38, 191–200.

Xu, H.F., Dong, Y.J., Shi, R.H., Jin, R.M., Shen, K., Li, X.G., 1992. The Granitoid–Greenstone Belts of Western Shangdong. Geological Publishing House, Beijing, pp. 1–83 (in Chinese with English abstract).

Xu, J.F., Castillo, P.R., Chen, F.R., Niu, H.C., Yu, X.Y., Zhen, Z.P., 2003. Geochemistry of late Paleozoic mafic igneous rocks from the Kuerti area, Xinjiang, northwest China: implications for backarc mantle evolution. Chem. Geol. 193, 137–154.

Zhai, M.G., Liu, W.J., 2003. Paleoproterozoic tectonic history of the North China Craton: a review. Precam. Res. 122, 183–199.

Zhao, G.C., Cawood, P.A., Lu, L.Z., 1999. Petrology and P–T history of the Wutai amphibolites: implications for tectonic evolution of the Wutai Complex, China. Precam. Res. 93, 181–199.

Zhao, G.C., Cawood, P.A., Wilde, S.A., Lu, L.Z., 2000. Metamorphism of basement rocks in the Central Zone of the North China Craton: implications for Paleoproterozoic tectonic evolution. Precam. Res. 103, 55–88.

Zhao, G.C., Sun, M., Wilde, S.A., Li, S.Z., 2003. Assembly, accretion and breakup of the Paleo-Mesoproterozoic Columbia Supercontinent: records in the North China Craton. Gondwana Res. 6, 417–434.

Zhao, G.C., Sun, M., Wilde, S.A., Li, S.Z., 2005. Late Archean to Paleoproterozoic evolution of the North China Craton: key issues revisited. Precam. Res. 136, 177–202.

Zhao, G.C., Wilde, S.A., Cawood, P.A., Lu, L.Z., 1998. Thermal evolution of the Archaean basement rocks from the eastern part of the North China Craton and its bearing on tectonic setting. Int. Geol. Rev. 40, 706–721.

Zhao, G.C., Wilde, S.A., Cawood, P.A., Sun, M., 2002a. SHRIMP U–Pb zircon ages of the Fuping complex: implications for late Archean to Paleoproterozoic accretion and assembly of the North China Craton. Am. J. Sci. 302, 191–226.

Zhao, G.C., Wilde, S.A., Cawood, P.A., Sun, M., 2001. Archean blocks and their boundaries in the North China Craton: lithological, geochemical, structural and P–T path constraints and tectonic evolution. Precam. Res. 107, 45–73.

Zhao, T.P., Zhou, M.F., Zhai, M.G., Xia, B., 2002b. Paleoproterozoic rift-related volcanism of the Xiong'er Group, North China Craton: implications for the breakup of Columbia. Int. Geol. Rev. 44, 336–351.